TRANSITION OF FREE CONVECTION FLOW BETWEEN TWO ISOTHERMAL VERTICAL PLATES

Ali S. Alzwayi and Manosh C. Paul[§]

Systems, Power & Energy Research Division, School of Engineering, University of Glasgow, Glasgow G12 8QQ, UK
[§]Corresponding author: Email: Manosh.Paul@glasgow.ac.uk, Tel: +44(0)141 330 8466, Fax: +44(0)141 330 4343

Abstract

Numerical simulations are performed to study the transition of the development of thermal boundary layer of air along isothermal heated plates in a large channel. In particular, the aim is to investigate the effects of the channel width on the transition of the flow under various plate temperatures. Realizable *k-ε* turbulence model with an enhanced wall function is employed to obtain the numerical simulations of flow and thermal fields in the channel. The channel width is varied from 0.04 m to 0.45 m and the numerical results of the maximum values of flow velocity, turbulent kinetic energy are recorded along the flow to examine the critical distance of the developing flow. Effects on the transition of the two different types of wall boundary conditions, isothermal and adiabatic, applied to the channel are also examined. The results particularly indicate that the flow transition in the isothermal cases takes later than that in the adiabatic cases.

Keywords: Free convection, Boundary layer, Laminar flow, Transition, Turbulent flow.

NOMENCLATURE

b	channel width
C_p	air specific heat capacity
g	gravitational acceleration
Gr	Grashof number = $g\beta(T_P - T_a)y^3/\nu^2$
h	heat transfer coefficient = $qp/(Tp - Ta)$
k	kinetic energy of turbulence
L	channel height
Nu	average of Nusselt number = $h\ b/\kappa$
n_y , n_x	number of nodes in the *y* and *x* directions respectively
p	pressure
Pr	Prandtl number
q_p	heat flux of the plate = $\int \frac{\partial T}{\partial x}\Big\vert_{x=0} dy$
T	temperature
u, v	velocity components in the *x* and *y* directions respectively
x, y	Cartesian coordinates

Greek Symbols

β	thermal expansion coefficient
Γ	exchange coefficient for general transport defined as μ/Pr

ρ	density
ν	kinematic viscosity
ε	dissipation rate of turbulent kinetic energy
μ	dynamic viscosity coefficient
μ_t	turbulent molecular viscosity
σ_t	turbulent Prandtl number
κ	thermal conductivity

Subscripts

a	air
P	plate
c	critical

1. Introduction

Over the recent years, more attention has been given to the natural convection as it naturally occurs in environment systems. Moreover, most practical and economical methods for developing a heating or cooling system use natural convection which is induced by buoyance forces with density gradient established thermally.

In 1942 the first experimental work on the buoyancy driven convection flow in a parallel walled vertical channel was done by Elenbaas [1] using air as a test fluid. Results were presented for a set of inclination angles of the plate varying from 0˚ to 90˚, and particular attention was given to the prediction of heat transfer coefficient. A good agreement was obtained between the theoretical and experimental data. One of his key findings was that the solution on the single plate would have to be approached for large plate spacing. Bodia and Osterle [2] later performed the first numerical simulation of buoyancy induced flow developing on a vertical channel. The governing equations were expressed in finite difference form and the walls were treated as isothermal. The air flow velocity and heat transfer coefficient were provided and validated with those of the theoretical and experimental data of Elenbaas [1]. Later, the numerical techniques of Bodia and Osterle [2] were widely used by many researchers to solve the free convection in vertical channel with different boundary and operating conditions, e.g. see the work presented in Miyatake and Fujii [3], Aung et al. [4] and Oosthuzien [5].

Streamwise development of the turbulent free convection flow between two vertical plates was experimentally investigated by Miyamoto et al. [6] and Katoh et al. [7]. The test fluid in this case was also air and different width of the channel was examined. In Miyamoto et al. [6] the channel was installed at various height from floor, e.g. 10, 90, 170 and 465 mm. The experimental data demonstrated that the heat transfer coefficients in the vertical heated plate of over 2 m long are almost independent to the height of the channel when it is positioned 10 mm above the floor. While, in Katoh et al. [7] a bell mouth was installed at the bottom of the channel, and for the heat transfer the comparison between the channel with a bell mouth and without it was done. The results showed that the heat transfer becomes smaller in the two cases.

Two-dimensional numerical simulations of turbulent natural convection in a heated channel were performed by Said et al. [8] and Badr et al. [9]. The governing equations were solved by

the finite volume discretisation method by assuming all the thermal properties of the air to be constant, except the density which was solved by the Boussinesq approximation.

In another recent study, thermal efficiency of flow in a vertical chimney (open ended channel) has experimentally been investigated by Burek and Habeb [10]. From the experimental data some correlations have been obtained to calculate the mass flow rate of air as well as temperature. The major finding has been that the mass flow rate is affected by both the channel depth and heat input to the system with the thermal efficiency remaining unaffected by the depth of the channel. Taofeek et al. [11], on the other hand, have used a Particle Image Velocimetry method to record turbulent characteristics of free convection in a channel with anti-symmetric heating. The data has been provided for two values of Rayleigh number, 1×10^8 and 2×10^8. The results indicated that the distributions of the velocity and temperature of the flow in this experimental model of the vertical channel are similar to those in a closed cavity. And, with increasing the Rayleigh number by 50%, the location of peak velocity moves close to the surface wall, which has close agreement with data recorded in a closed cavity.

As seen, all these experimental or numerical studies mainly focused on the investigation of the behaviour and characteristics of free convection flow inside a channel under different boundary and operating conditions. And most of them were carried out either on laminar or turbulent flow and hence neglected transition. But most recently Alzwayi and Paul [12] and Alzwayi and Paul [13] provided numerical results on the flow transition inside a channel where one of the heated plates in the channel was kept isothermal and the other one, placed opposite to it, was adiabatic. However, very little is known about the transition stage in a vertical channel when the two heated plates are kept under an isothermal condition. Moreover, when free convection occurs relatively in a large scale, little reliable information can be obtained from an experimental / laboratory based experiment, and in some cases undertaking various experimental tests e.g. with varying the channel width and operating as well boundary conditions may be difficult and a costly process. The key objective of this work is therefore to perform a series of numerical examination to investigate the natural convection flow developing between two isothermal plates and then examine the transition of this flow with a particular attention paid to the interaction which will occur between the thermal boundary layers separating from each heated plate. Furthermore, effects on the transition stage occurring between the two-flow conditions of a channel (isothermal and adiabatic) are also investigated.

2. Model Geometry

The channel is formed by two vertical plates with length L, and the distance separating them is denoted by b. Both the plates (left and right) are kept at an isothermal condition. The numerical simulations are considered to be two-dimensional, incompressible, Newtonian, free-convection and steady state. The air with a Prandtl number of 0.7 is chosen to be the test fluid. The model geometry along with the Cartesian coordinate system is shown Figure 1 which has the same schematic drawing as in Alzwayi and Paul [12].

3. Mathematical Formulation

3.1. Governing Equation

The conservation equations of mass, momentum and energy for a two-dimensional incompressible fluid flow are respectively written in the following forms:

$$\frac{\partial(\rho u)}{\partial x}+\frac{\partial(\rho v)}{\partial y}=0\,, \tag{1}$$

$$\frac{\partial(\rho uu)}{\partial x}+\frac{\partial(\rho uv)}{\partial y}=-\frac{\partial P}{\partial x}+\frac{\partial}{\partial x}\left(\mu\frac{\partial u}{\partial x}\right)+\frac{\partial}{\partial y}\left(\mu\frac{\partial u}{\partial y}\right), \tag{2}$$

$$\frac{\partial(\rho vu)}{\partial x}+\frac{\partial(\rho vv)}{\partial y}=-\frac{\partial P}{\partial y}+\frac{\partial}{\partial x}\left(\mu\frac{\partial v}{\partial x}\right)+\frac{\partial}{\partial y}\left(\mu\frac{\partial v}{\partial y}\right)+g\left(\rho-\rho_0\right), \tag{3}$$

$$\frac{\partial(\rho uT)}{\partial x}+\frac{\partial(\rho vT)}{\partial y}=\frac{\partial}{\partial x}\left(\Gamma\frac{\partial T}{\partial x}\right)+\frac{\partial}{\partial y}\left(\Gamma\frac{\partial T}{\partial y}\right). \tag{4}$$

These equations are solved directly (subject to the boundary conditions described below) for the natural convection flow in laminar region, while in turbulent region both the Γ and μ terms are replaced by their effective values defined by $\mu_{eff} = \mu + \mu_t$ and $\Gamma_{eff} = \mu/Pr + \mu_t/\sigma_t$ respectively.

In the recent study, Alzwayi and Paul [12] have examined that the Realizable k-ε turbulent model of Shih et al. [14] performs best in predicting the transition of the free convection flow over a vertical channel, compared to the other two well-known models such as the standard and RNG k-ε models. Therefore, this model is particularly chosen in the present study to determine the turbulent viscosity μ_t which depends on the turbulent dissipations energy, ε, and the turbulent kinetic energy, k. The turbulent viscosity μ_t , also known as the eddy viscosity of turbulent flow, depends on the mean flow rate of the deformation from the Boussinesq theory. A time averaging is carried out to the above governing equations (1) – (4) to obtain the Reynolds averaged Navier-Stokes (RANS) equations which are solved by using the Realizable k-ε model. However, these equations contain unknown Reynolds stresses which are expressed as the deformation of the mean flow quantises, for example, for the momentum equations these can be written as $\tau_{ij} = -\rho\overline{u_i'u_j'} = \mu_t\left(\frac{\partial u_i}{\partial x_j}+\frac{\partial u_j}{\partial x_i}\right)$, where, τ_{ij} are the shear stresses, u' is the velocity fluctuation in the turbulent flow. The k and ε equations for the Realizable model [14] are written as

$$\frac{\partial(\rho uk)}{\partial x}+\frac{\partial(\rho vk)}{\partial y}=\left[\left(\mu+\frac{\mu_t}{\sigma_k}\right)\frac{\partial k}{\partial x}\right]+\frac{\partial}{\partial y}\left[\left(\mu+\frac{\mu_t}{\sigma_k}\right)\frac{\partial k}{\partial y}\right]+G_k+G_b-\rho\varepsilon \tag{5}$$

$$\frac{\partial(\rho u\varepsilon)}{\partial x}+\frac{\partial(\rho v\varepsilon)}{\partial y}=\frac{\partial}{\partial x}\left[\left(\mu+\frac{\mu_t}{\sigma_\varepsilon}\right)\frac{\partial\varepsilon}{\partial x}\right]+\frac{\partial}{\partial y}\left[\left(\mu+\frac{\mu_t}{\sigma_\varepsilon}\right)\frac{\partial\varepsilon}{\partial y}\right]+$$
$$\rho C_1S_\varepsilon-\rho C_2\frac{\varepsilon^2}{\varepsilon+\sqrt{\nu\varepsilon}}+G_{1\varepsilon}\frac{\varepsilon}{k}C_{3\varepsilon}G_b \tag{6}$$

where, $C_1=\max[0.43,\eta/(\eta+5)]$ and $\eta=Sk/\varepsilon$. The eddy viscosity is then computed by $\mu_t=\frac{\rho k^2}{\varepsilon}\left(A_0+A_S\frac{kU^*}{\varepsilon}\right)^{-1}$ with A_0 = 4.04 and $A_s=\sqrt{(6cos\emptyset)}$ where $\emptyset=1/3\,cos^{-1}\left(\sqrt{6}W\right)$. The formulation of U^* and W depend on the angular velocity [14], and G_k and G_b reflect the rate and generation of the turbulent kinetic energy respectively and determined by

$$G_k=\mu_t\left(\frac{\partial u_i}{\partial x_j}+\frac{\partial u_j}{\partial x_i}\right)\frac{\partial u_i}{\partial x_j}-\frac{2}{3}\rho k\delta_{i,j}\frac{\partial u_i}{\partial x_j}\,,\qquad G_b=g_i\beta\frac{\mu_t}{\sigma_t}\frac{\partial T}{\partial x_j}$$

where g_i *is* the gravitational vector acting in the direction j, β is the thermal expansion coefficient of air defined as $\beta=-\frac{1}{\rho}\left(\frac{\partial\rho}{\partial T}\right)_{p_{constant}}$. The model constants used in the simulations are $C_{1\varepsilon}$ = 1.44, C_2 = 1.9, $C_{3\varepsilon}$ = 1.0, σ_k = 1.0 and σ_ε = 1.2 [14].

3.2. Boundary Conditions

No slip boundary condition is imposed on the velocity components at the both walls for which we set $u_i = 0$. The temperature (*Tp)* of the heated plate situated on the left hand side of the channel will be fixed to 70°C, while the temperature of the plate opposite to it will be varied according to the boundary condition described in equation (8). Moreover, the air / ambient temperature (*Ta*) will be fixed to 15°C.

$$T = Tp, \quad \text{for} \quad 0 \le y \le L, \qquad x = 0 \tag{7}$$

$$T = Tp^*, \quad \text{for} \quad 0 \le y \le L, \qquad x = b \tag{8}$$

Turbulent kinetic energy vanishes at the walls so we set $k = 0$. Since the distributions of the characteristics of flow have a large gradient near the walls, an enhanced wall function is also used as the wall boundary condition. Moreover, the inlet boundary is subject to the ambient conditions, while at the outlet the static gauge pressure is set to zero. The choice of these boundary conditions used at the inlet and outlet of the channel was examined through a set of trial simulations using a large area attached to the inlet as well as to the outlet of the channel (as in the recently published work of Terekhov and Ekaid [15] and Lau et al. [16]). Figure 2 clarifies that the induced flow velocity distribution close to the inlet (y =0.09m) differs due to the large area added before the inlet. But, the effect almost disappears as the flow develops along the large channel. The development of thermal boundary layer, as evidence by the temperature plots in the frames right hand side of the figure, shows no (major) influence when the large area was added to the inlet. It was understood from this investigation that the induced flow in a tall vertical channel hardly changes except very close to the inlet section, which is expected.

We note that the effect of different boundary conditions in a large channel was investigated both experimentally and numerically by Katoh et al. [7] and Ben-Mansour et al. [17]. Katoh et al. [7] installed a bell mouth entrance at the channel inlet to control the inlet flow and their results indicated that the general characteristics of the profiles of temperature and vertical velocity are similar to those obtained by without the bell mouth. Whereas Ben-Mansour et al. [17] studied the effect of four different inlet and outlet boundary conditions (e.g. uniform pressure at the inlet and outlet, extended inlet and extended outlet, radial flow inlet and radial flow outlet, and uniform velocity at inlet and outflow condition at exit). Their results also showed that the uniform pressure inlet condition exhibits results which are in very close agreement with experimental data.

3.3. Numerical techniques and grid resolution study

The numerical methods used to solve the governing equations have already been described in more details in Alzwayi and Paul [12] and validated with suitable experimental data in a vertical heated channel. The code uses finite volume technique for the discretisation of the governing equations with a second order upwind scheme to solve these discretised equations, where the unknown quantities at the cell faces are computed by using a multidimensional linear reconstruction approach described in Barth and Jespersen [18] to achieve higher order at the cell faces through a Taylor series expansion of the cell cantered solution about the cell centroid. The SIMPLE algorithm of Patankar [19] is employed to solve the pressure based equation which is derived from the momentum and continuity equations such that the velocity and pressure fields are coupled to each other and solved by adopting an iterative solution strategy explained in [12]. Final converged numerical solutions are achieved when the residuals of the continuity and velocity components become less than 10^{-6}. The residual of the energy, turbulent kinetic energy and its dissipation is reduced to 10^{-8} to avoid any sensitivity to the solutions of the turbulent fluctuating components.

An in-depth investigation on the grid resolution has been carried out by using six different grids (22 × 220, 30 × 370, 120 × 370, 200 × 370, 300 × 370 and 200 × 400) with a fine resolution of mesh clustered at the middle of the channel as presented in Figure 3 . The variation found in the simulation results predicted by the last four grids was very small and almost negligible. Therefore, as in the previous studies, e.g. Alzwayi and Paul [12] and Alzwayi and Paul [13], the grid size of 200 × 370 is chosen to avoid any undesirable discrepancies in the numerical results and at the same time to save the computational time to perform all the numerical simulations.

4. Results and discussions

4.1. Flow feature: an overview

In order to determine the influence of the channel width on the development of the boundary layers of flow, variation of the axial profiles of temperature, turbulent kinetic energy and velocity across the channel width are presented in this section. The results are reported at different vertical locations: y = 0.5 m, 1.5 m, inlet and outlet, while the width (b) of the channel is varied from 0.04 m to 0.3 m.

In the first case, the plate located at the right hand side of the channel is kept at a temperature Tp^* = 40°C and the inlet temperature is fixed at 15°C. Variation of the heated air temperature, determined by $dT = (T-Ta)/(Tp-Ta))$ and presented in Figure 4, shows an increase in the temperature due to the air heated up by the heat transfer which convects downstream of the channel. However, the outlet temperature of the channel drops as the width of the channel is increased due to the fact that the thermal boundary layer grows in a wider space available inside the channel. And the temperature difference between the outlet and the inlet becomes very small with an increase in the channel width as shown in Figure 4 (e, f). However, when $b \geq 0.08$ m, the temperature around the channel centreline (e.g. at $x = b/2$) and at the middle of the channel (y = 1.5 m) becomes equal to the ambient temperature as a result of the more space available for the development of flow.

Distribution of the turbulent kinetic energy is reported in Figure 5. The magnitude of the turbulent kinetic energy at b = 0.04 m is larger compared to that found in the other cases except at the outlet section for b = 0.3 m, which is a result of the strong interaction of the two boundary layers developed in a relatively small space inside the channel. In all the cases, the peak of the turbulent kinetic energy near the right wall of the channel at y = 0.5 m is larger than that occurring at the left wall. The phenomena are explained by the fact that the magnitude of the velocity (shown in Figure 6) adjacent to the right plate drops, which causes a flow deceleration and results in an increase in the turbulent kinetic energy near the right wall. But with an increase in the width of the channel, e. g. when $b \geq 0.1$ m, the effect of the buoyancy force on the left wall becomes more evident, where the turbulent kinetic energy reaches its peak near the left wall of the channel.

The variation of the velocity across the channel is shown in Figure 6. As can be seen, with an increase in the channel width the mean velocity of air drops across the channel. The velocity profiles at the inlet section are more affected by the high viscous force compared to the buoyancy force near the heated plate, and the velocity profiles at the downstream (0.5 m $\leq y \leq$ 1.5 m) become flat in the middle of the channel.

Further to note in Figure 6 (a-d) that the peak of the outlet velocity in a small width of the channel, e.g. when 0.04 m ≤ b ≤ 0.1 m, it is found to be slightly lower than that at the middle of the channel (at y = 1.5 m). This is occurring due to the fact that the flow starts to development in the middle of the channel and the buoyancy force accelerates the fluid inside the channel with an increase in the thickness of the two boundary layers in a small space, which leads to decrease the velocity at the outlet section.

4.2. Effects of the boundary conditions

In the previous section typical results of the flow velocity and temperature have been presented and discussed, where the effect of the channel width has been investigated for a particularly chosen plate temperature, Tp^* = 40°C. This temperature will now be changed to 70°C and the results will be compared with those obtained by Tp^* = 40°C as well as by the adiabatic case studied in Alzwayi and Paul [12]. As already seen in Figure 7, the velocity profile has been mostly affected by the buoyancy force, with a peak appeared near each of the heated plates.

In this section we will focus on the examination of the velocity peak particularly at y = 1.5 m and 3 m. Only the velocity peak near the left heated wall is used, as in the adiabatic case we obtained a single velocity peak (e.g. see Alzwayi and Paul [12]). We also note that the value of the two velocity peaks on the two channel sides in the isothermal case of Tp^* = 70°C is equal.

Figure 7 shows the value of the peak velocity profiles and its location obtained by the three different boundary conditions: Tp^* = 40°C, Tp^* = 70°C and adiabatic. Figure 7 (a) generally shows a larger variation in the peak velocity at y = 1.5 m than that at the outlet section due to the flow developing in the middle of the channel. In the channel outlet, Figure 7 (b) shows that the variation only appears for the small channel width when b ≤ 0.1 m. In addition, the velocity peaks for the two isothermal cases are same because the flow becomes fully developed at the outlet section, but they are still larger than those for the adiabatic case in the range of channel width b ≥ 0.15 m due to the buoyancy force which is higher in the isothermal cases than that in the adiabatic case.

The location of the velocity peak is also presented in Figure 7 (c, d). It is clearly seen that the peak velocity of the flow appears to move towards the heated plate when the channel width is increased. In addition, the peak velocity in the adiabatic case becomes very close to the heated wall compared to that in the isothermal cases. However, the velocity peaks at y = 3.0, Figure 7 (d), moves nearer the heated plate compared to y = 1.5 m in Figure 7 (c) since the flow is fully developed at the outlet of the channel.

The air velocity and temperature at the outlet are now summarised in Figure 8. In order to make a direct comparison of these with those obtained by the adiabatic case, a percentage of increment is calculated by using $dv_{inc} = (v_{out\ iso} - v_{out\ adi})/(v_{out\ adi})*100$ for the velocity magnitude. The same approach is used for the determination of temperature increment. As can now be seen in Figure 8 (a) that the outlet velocity grows with the channel width for the isothermal cases as a result of an increase in the buoyancy force in the convection flow. But, after reaching a peak at around b = 0.3 m, the velocity drops for the large width of the channel. The air velocity has an impact on the flow temperature and the results plotted in

Figure 8 (b) show an opposite effect, i.e. the added heated temperature drops with the channel width to a minimum followed by an increase for the large width.

4.3. Boundary layer growth: isothermal vs. adiabatic cases

Effect of the width of the channel on the growth of the boundary layers along the flow is summarised here with the distributions of the maximum velocity, turbulent kinetic energy and turbulent intensity determined by using $f_{\max}(y) = \underset{x\min \le x \le x\max}{Max} f(x,y)$, where f is a generic variable, and plotted in Figure 9. Comparison is made between the results of the adiabatic and isothermal cases, and the temperature of the plate on the right hand side of the channel for the isothermal case is kept at $Tp_* = 40°C$.

The results presented in Figure 9 indicate that the velocity magnitude in the isothermal case is generally higher than that of the adiabatic case due to the increase in the buoyancy force mentioned earlier. And, particularly, in the isothermal cases for b = 0.04 m to 0.10 m, the velocity distribution approximately becomes constant as shown in Figure 9 (a) when $y \le 1.5$ m. While, in the adiabatic cases the distribution of the velocity show a magnitude drop from the peak towards the downward. However, for the rest of channel width e.g. b = 0.15 m to 0.45 m, as in Figure 9 (b), both the cases show a similar behaviour with a shift in the velocity profile towards the downstream for the isothermal cases. In both the cases the maximum velocity at the outlet section has an approximately same magnitude which is ≈ 0.8 m/s.

Figure 9 (c-d) presents the maximum turbulent kinetic energy inside the channel. For a small width of the channel, e.g. when b = 0.04 m and 0.06 m, the kinetic energy in the isothermal case is larger than that of the adiabatic case, which is expected as in the isothermal case there is a strong interaction occurring between the two boundary layers within a relatively small distance. However for $b \ge 0.10$ m, the distribution of the kinetic energy in the adiabatic case is larger than that of the isothermal case due to the fact that a single boundary layer which grows in the adiabatic case gets enough space in the channel to develop fully, whereas in the isothermal case an interaction between the two boundary layers occurs.

The distribution of the turbulent intensity presented in Figure 9 (e, f) has a similar profile as the turbulent kinetic energy. When $b \ge 0.1$ m, the turbulent intensity in the isothermal case is smaller than that of the adiabatic case. The turbulent intensity also increases sharply towards the downstream, especially at the outlet of the channel, due to the turbulent nature of the flow occurring at the downstream regime.

Contours of the turbulent kinetic energy, turbulent intensity and velocity inside the channel are shown in Figure 10 (A), (B) and (C) respectively for the different channel width: 0.05 m, 0.1 m, 0.15 m, 0.2 m, 0.3 m and 0.45 m. To make a direct comparison between the adiabatic and isothermal cases the contours are plotted pairwise in frames (a, c, e, g, i, k) for the adiabatic cases and in (b, d, f, h, j, l) for the isothermal cases. In general, the contour plots show that the maximum turbulent kinetic energy and its turbulent intensity in the isothermal cases dropped by 41% and 20% respectively compared to the adiabatic cases. This is related to the interaction occurring between the two boundary layers in the isothermal case, clearly seen in frames (h, j and l) when $b \ge 0.2$ m. While in the adiabatic case only one boundary

layer grows on the left hand side with an ample space to fully develop as seen in frames (i) and (k).

4.4. Flow transition

As seen in Figure 10 (A), (B) and (C) the boundary layer in the isothermal cases grows on the both sides of the channel and a separation / transition occurs from the laminar to turbulent stage towards the channel downstream. In this section the transition behaviour will be examined by taking into account of the distribution of the maximum velocity on the left ($0 \leq x \leq b/2$) and right ($b/2 \leq x \leq b$) hand sides of the channel.

Figure 11 (a) and (b) initially show the maximum velocity field obtained in the left and right side domains, where the temperature of the heated plates is kept as 70°C and 40°C respectively. The maximum velocity on both sides of the channel is same at the upstream near the inlet where the effect of the buoyancy force on the velocity field is expected to be similar.

As the distribution of the peak velocity is considered to be a starting point of the flow transition, Figure 11 (a) shows that the transition point of the flow developing on the left hand side of the wall for the cases when $b \leq 0.10$ m appears to be within the range $1.0 \leq L_c \leq 1.8$ m. However, the distribution of the velocity on the right hand side has a different behaviour, which shows a continued drop in magnitude after a slight increase near the inlet when $b \leq 0.1$ m due to the strong interaction occurred between the two boundary layers, already explained in Figure 10 (b-d). These results are however unable to determine the transition point on the right hand side and it is still more affected by the left hand side of the channel wall.

However, Figure 11 (b) shows that the velocity in the right wall increases to a peak at the transition point when $b \geq 0.15$ m because there is now enough space available for the development of flow. However, the location of the flow transition point on the right side is higher than that on the left side. Moreover, the thickness of the boundary layer on the right hand side is small and the flow becomes more stable which causes a delay in the transition process.

Finally, the transition of the flow boundary layers on the left and right hand sides of the channel are summarised in Figure 12 in terms of their critical distance obtained from the velocity results shown in Figure 11. Comparison of the two isothermal and the adiabatic cases is also given.

As can be noticed in Figure 11 (a) that it is very difficult to estimate the transition point on the right hand side of the channel with a small width e.g. when $b \leq 0.08$ m due to the strong interaction occurred between the two boundary layers (Figure 10 (b)). However, with an increase in the channel width, e.g. when $b \geq 0.1$ m, the transition on the right side wall appears late compared to that in the left hand side; this is expected as the temperature in the right side is lower than that of the left side. Also, when $Tp^* = 70$°C both the sides of the channel are kept at under the same isothermal condition, and that is why only the results obtained from the right side of the channel are reported in the comparison. Further, with an increase in the channel temperature, the flow inside the channel becomes unstable early as the critical distance drops and therefore an early transition occurs. Particularly, for a relatively

small channel width, e.g. when b = 0.04 m, the transition of the flow appears to be very quick.

5. Conclusion

Effects of the wall temperature of the parallel-plate channel and its width on the developing free-convection flow have been investigated numerically under the various operating and geometrical conditions. Two vertical plates of the channel are kept under the isothermal conditions, and the distance separating the two parallel plates is systematically reduced from 0. 45 m to 0.04 m to examine the flow separation, and consequently, their process of transition.

The results indicated that with an increase in the channel width, the location of the velocity peaks moved very close to the heated plate. This was particularly noticeable for the cases with relatively a small channel width.

At the transition stage, however, the results show that the flow transition in the adiabatic case takes early compared to that in the isothermal cases due to the single boundary layer which developed along the heated plate. On the other hand, a late transition occurs when the two heated plates are kept under the isothermal condition. Moreover, with an increase in the average channel temperature in the isothermal cases, the boundary layer on each side of the channel grows early and the flow becomes unstable due to the consequences of the shorter laminar region and the turbulent flow which develops early.

Acknowledgements

The authors thank the anonymous reviewers for their valuable comments and constructive suggestions on the earlier version of this paper, which have helped them to improve the manuscript. We also thank Dr D. A. S. Rees at the University of Bath for helpful discussion with him on the various aspects of the numerical results.

References

[1] W. Elenbaas, *Heat dissipation of parallel plates by free convection*, Laboratoria, N. V. Philips, (1942) 1-28.

[2] J.R. Bodia, J.F. Osterle, The development of free convection between heated vertical plates. *Journal of Heat Transfer*, 84 (1962) 40-44.

[3] O. Miyatake, T. Fujii, Free convective heat transfer between vertical plates-One plate isothermally heated and the other thermally insulated, *Heat Transfer-Japanese Research*, 1 (1972) 30-38.

[4] W. Aung, L.S. Feletcher, V. Sernas, Developing laminar free convection between vertical flat plates with asymmetric heating. *International Journal of Heat and Mass Transfer*, 15 (1972) 2293-2308.

[5] P.H. Oosthuzien, A numerical study of laminar free convection flow through a vertical open heated plane duct. *Fundamentals on Natural Convection - Electronic Equipment Cooling,* 32 (1984) 41-48.

[6] M. Miyamoto, Y. Kato, J. Kurima, Turbulent free convection heat transfer from vertical parallel plates in air, NII - Electronic Library service, the Japan Society of Mechanical Enginners, 34 (1983) 1-7.

[7] Y. Katoh, M.Miyamoto, J. Kurima, S. Kaneyasu, Turbulent free convection heat transfer from vertical parallel plates, *JSME International Journal*, 34 (1991) 496-501.

[8] S. A. M. Said, A. Habeb, H. M. Badr, S. Anwar, Numerical investigation of natural convection inside an inclined parallel walled channel, *International Journal for Numerical Methods in Fluids*, 49 (2005) 569-582.

[9] H. M. Badr, M. A. Habib, S. Anwar, Turbulent natural convection in vertical parallel-plate channels, *Heat and Mass Transfer*, 43 (2006) 73-84.

[10] S.A.M. Burek, A. Habeb, Air flow and thermal efficiency characteristics in solar chimneys and Trombe Walls, *Energy and Building*, 39 (2007) 128-135.

[11] F. Taofeek, T. F. Ayinde, S. A. M. Said, M. A. Habib, Turbulent natural convection flow in a vertical channel with anti-symmetric heating. *Heat and Mass Transfer*, 44 (2008) 1207-1216.

[12] A. S. Alzwayi, M. C. Paul, Effect of width and temperature of a vertical parallel plate channel on the transition of the developing thermal boundary layer, *International Journal of Heat and Mass Transfer*, 63 (2013) 20- 30.

[13] A. S. Alzwayi, M. C. Paul, Transition of free convection flow inside an inclined parallel walled channel: effects of inclination angle and width of the channel, *International Journal of Heat and Mass Transfer*, 68 (2014) 194-202.

[14] T, H. Shih, W. W. Liou, A. Shabbir, Z.Yang, J. Zhu, A new k-ε eddy viscosity model for high Reynolds number turbulent flows, *Computers and Fluids*, 24 (1995) 227-238.

[15] V.I. Terekhov and A.L. Ekaid, Turbulent free convection between vertical isothermal plates with asymmetrical heating, *Thermophysics and Aeromechanics*, 2013, Vol. 20, No. 2, 151-162.

[16] Lau et al., Numerical and experimental investigation of unsteady natural convection in a vertical open-ended channel, *Computational Thermal Sciences*, Volume 4, 2012 Issue 5, 443-456.

[17] Ben-Mansour et al., Comparison of different turbulent models and flow boundary conditions in predicting turbulent natural convection in a vertical channel with isoflux plates, *The Arabian Journal for Science and Engineering*, 2006, Vol. 32, pp. 191-218.

[18] T.J. Barth, D. Jespesen, The design and application of upwind schemes on unstructured meshes, Technical report AIAA-89-0366, Aerospace sciences meeting , Reno, Nevada, 1989.

[19] S.V. Patankar, Numerical Heat Transfer and Fluid Flow. Hemisphere Publishing Corporation, New York, 1980.

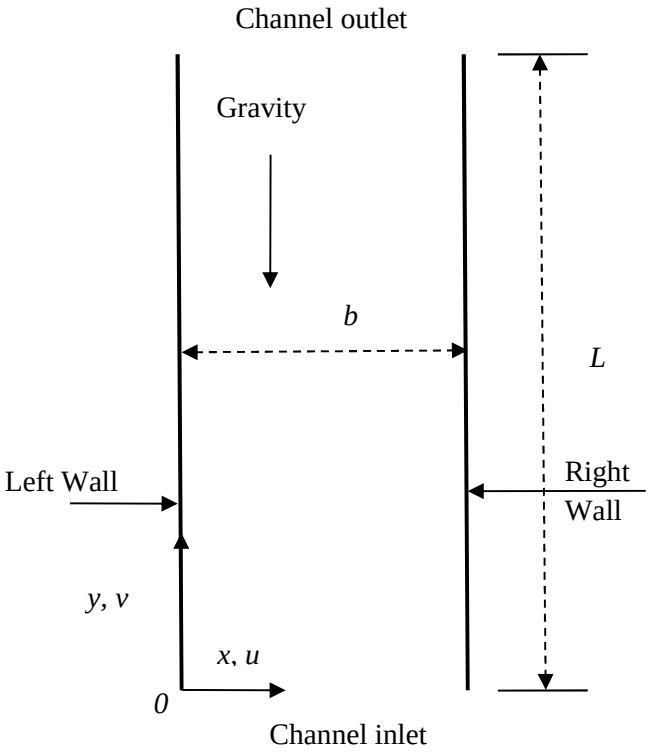

Figure 1 Schematic of a vertical parallel plate channel.

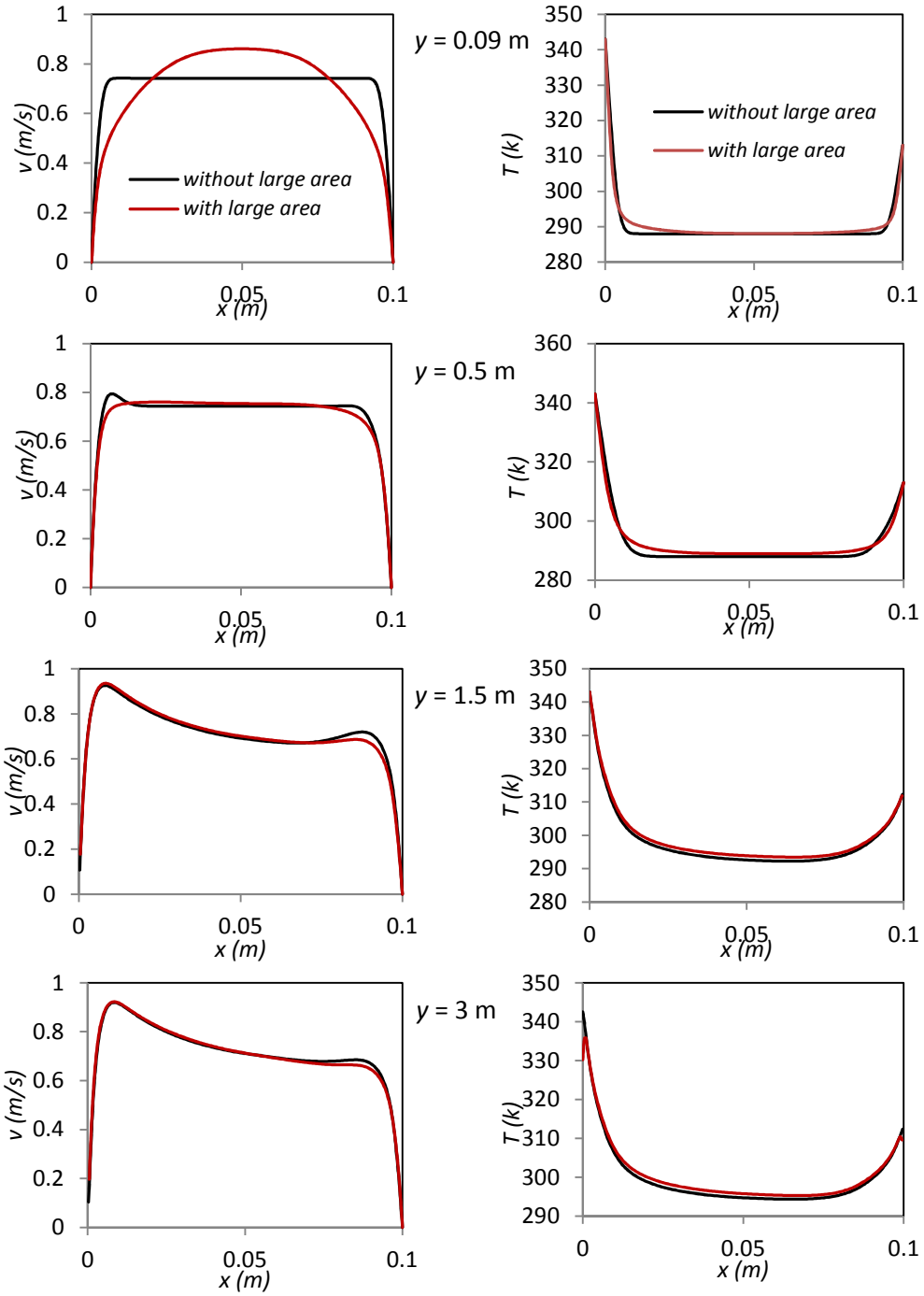

Figure **2**: Induced velocity (left) and temperature (right) distributions across the channel plotted at various location of *y*.

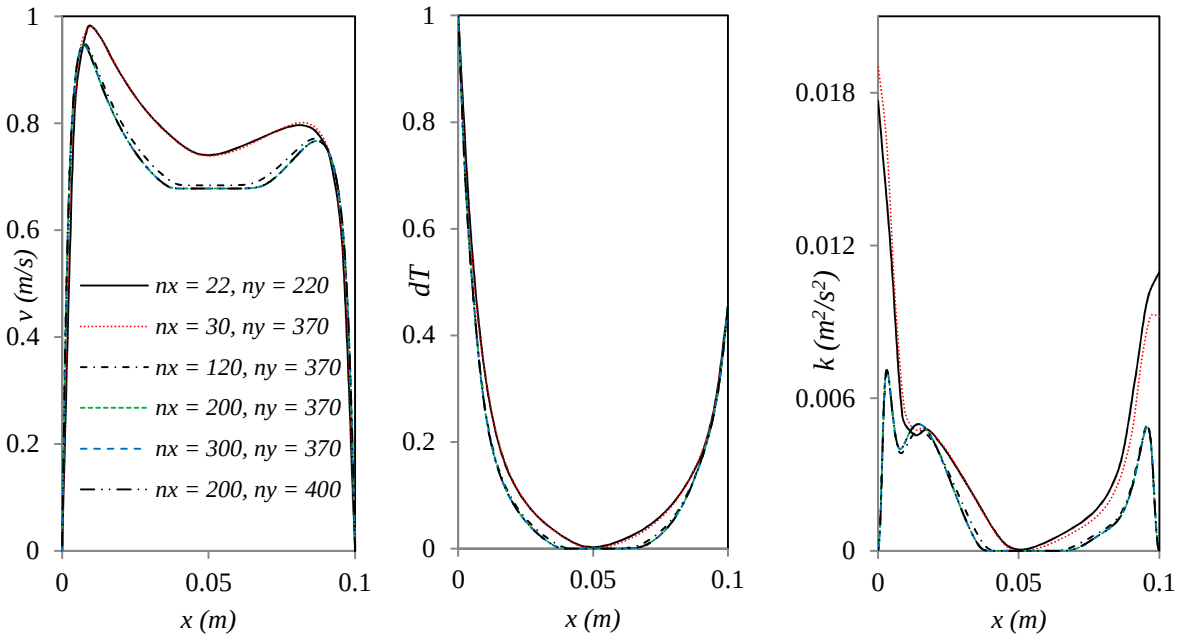

Figure 3 Mesh dependence test showing on the results of velocity, temperature and turbulent kinetic energy.

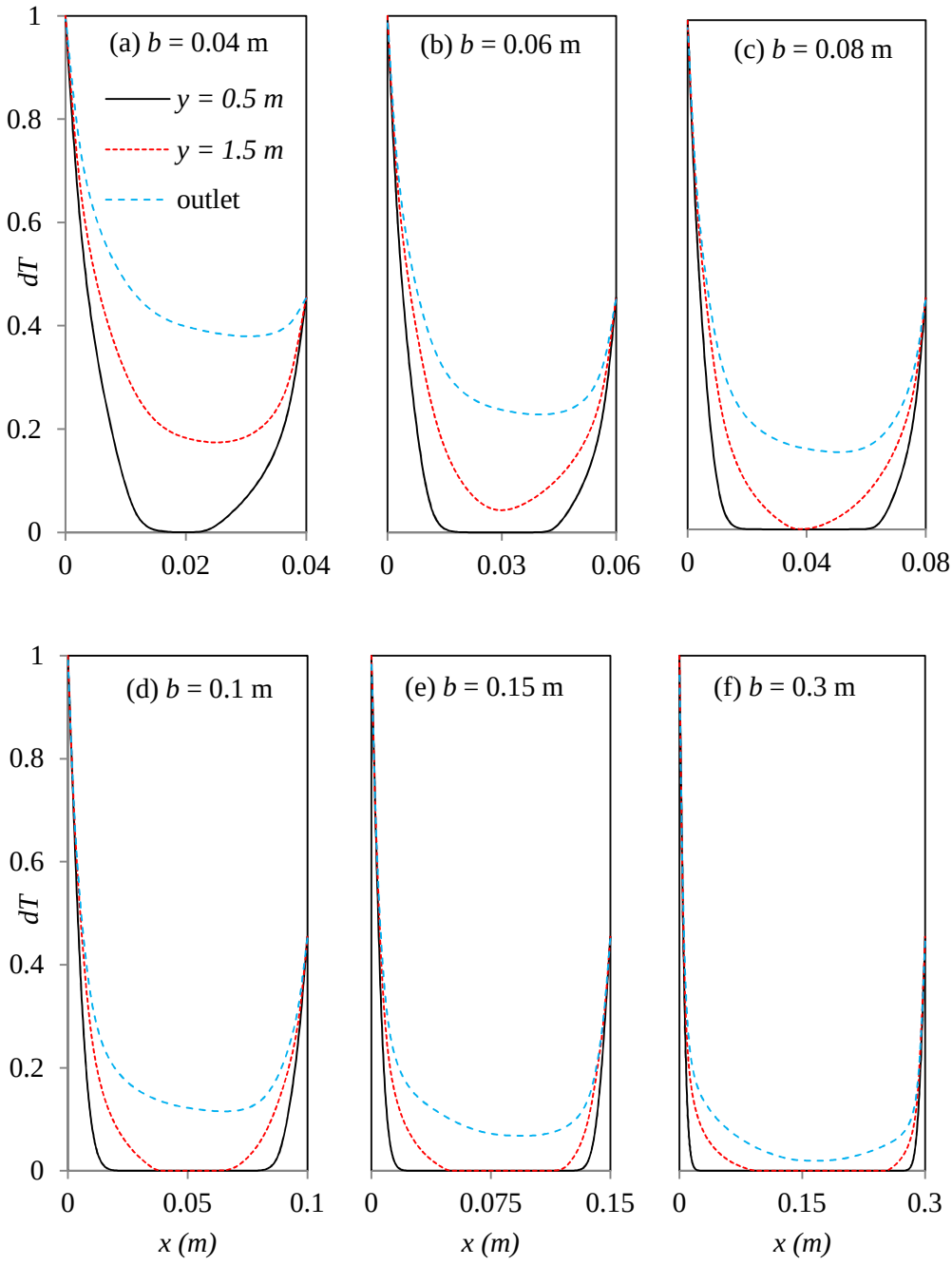

Figure 4 Effects of the channel width on the temperature at Tp^* = 40°C.

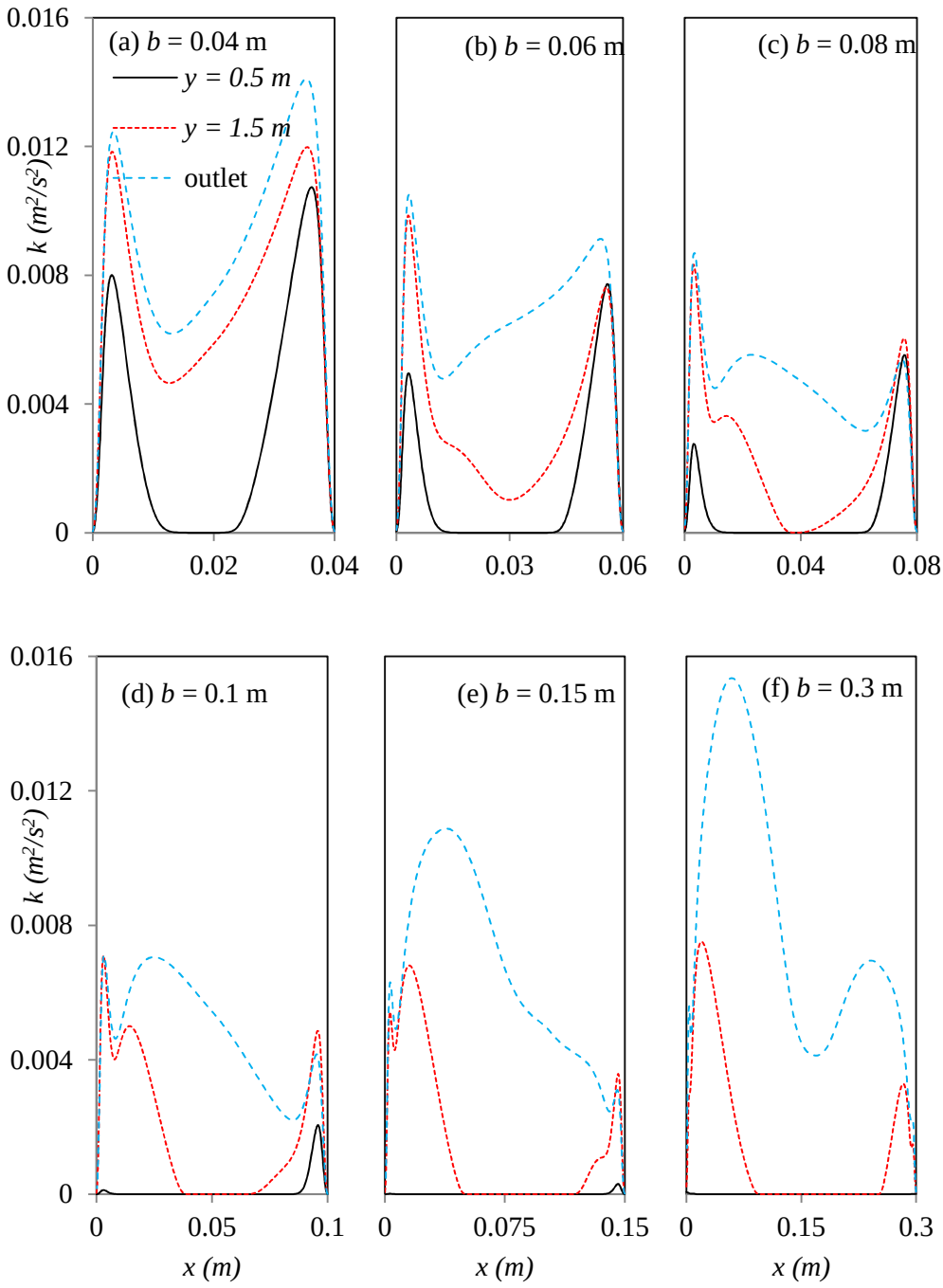

Figure 5 Effects of the channel width on the turbulent kinetic energy at Tp^* = 40°C.

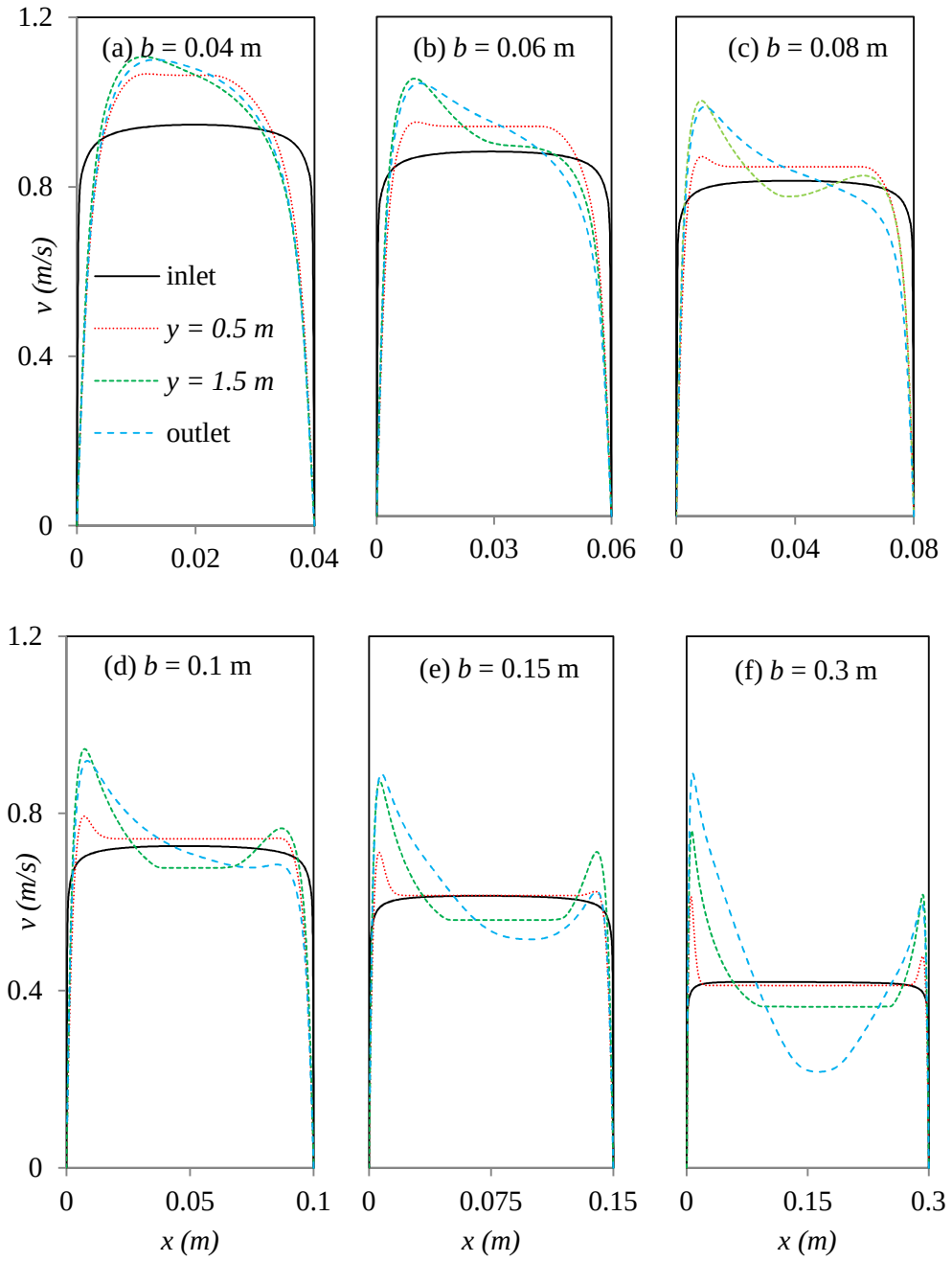

Figure 6 Effects of the channel width on the velocity of air at Tp^* = 40°C.

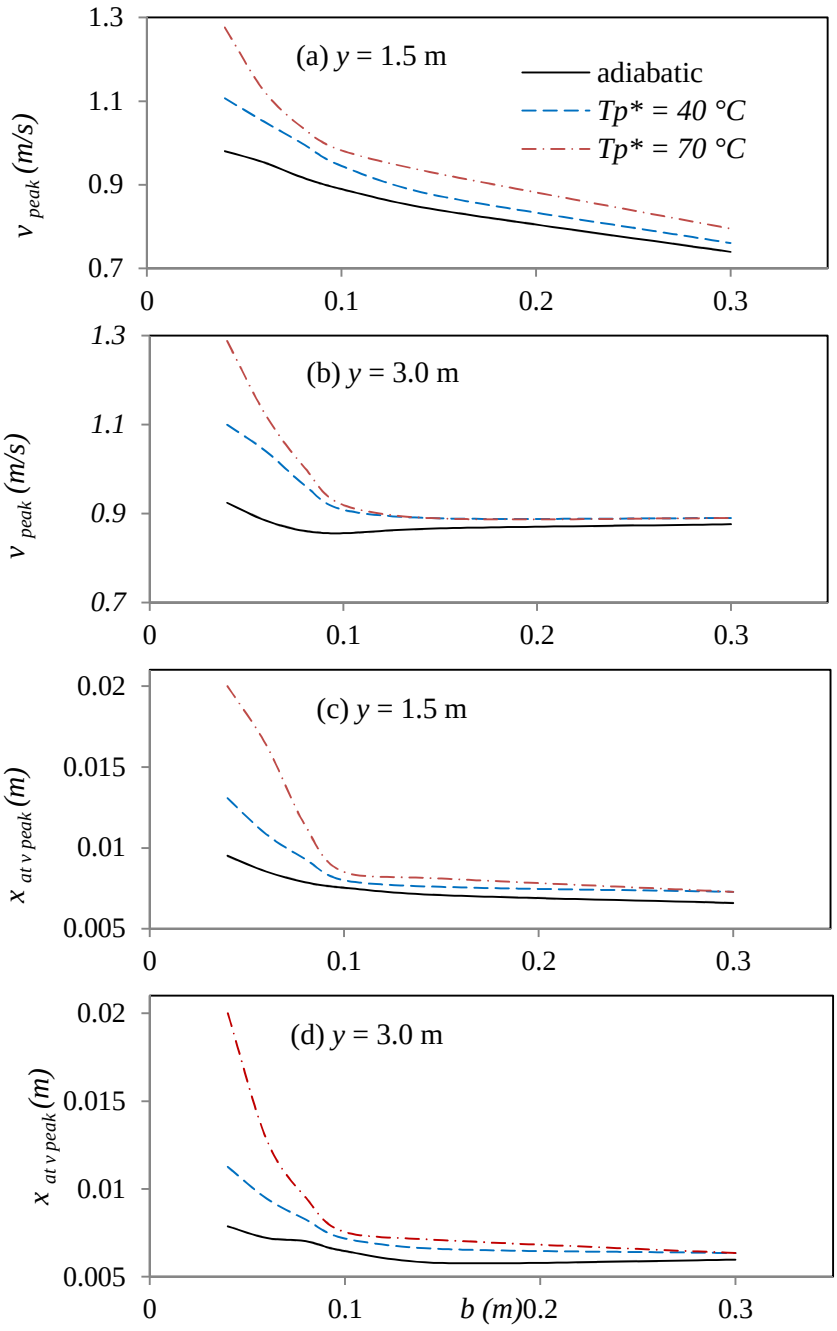

Figure 7 Peak velocity (a, b) and its location (c, d).

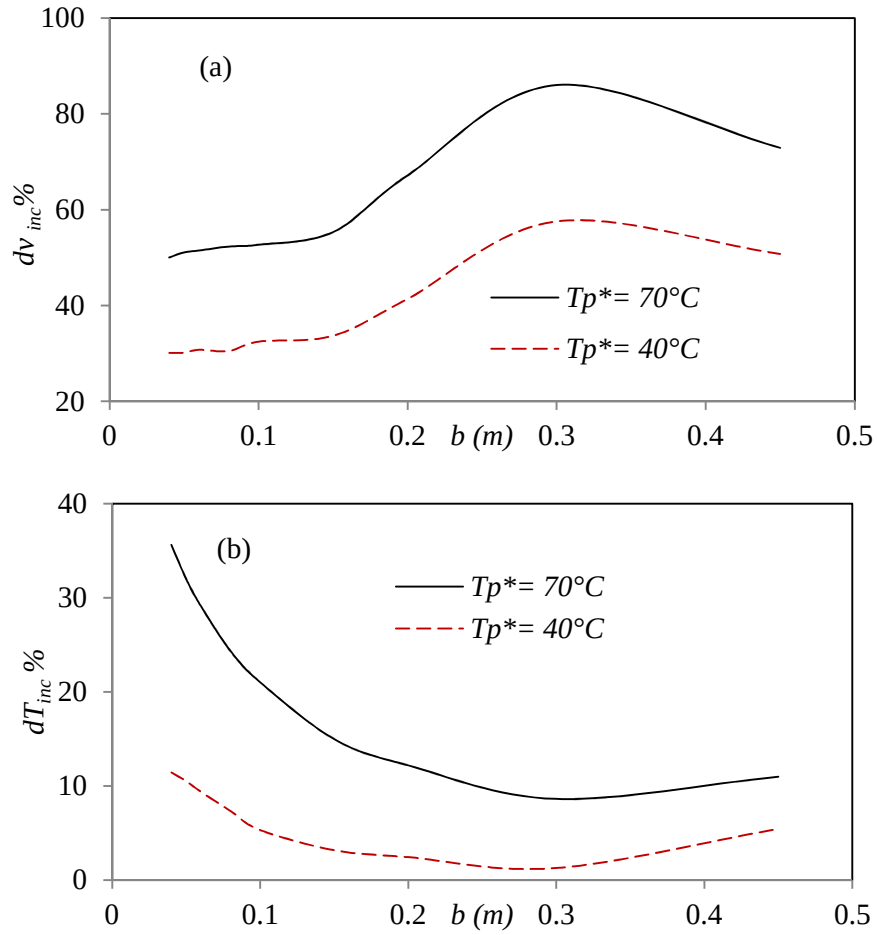

Figure 8 Increment of velocity (a) and temperature (b) at the outlet.

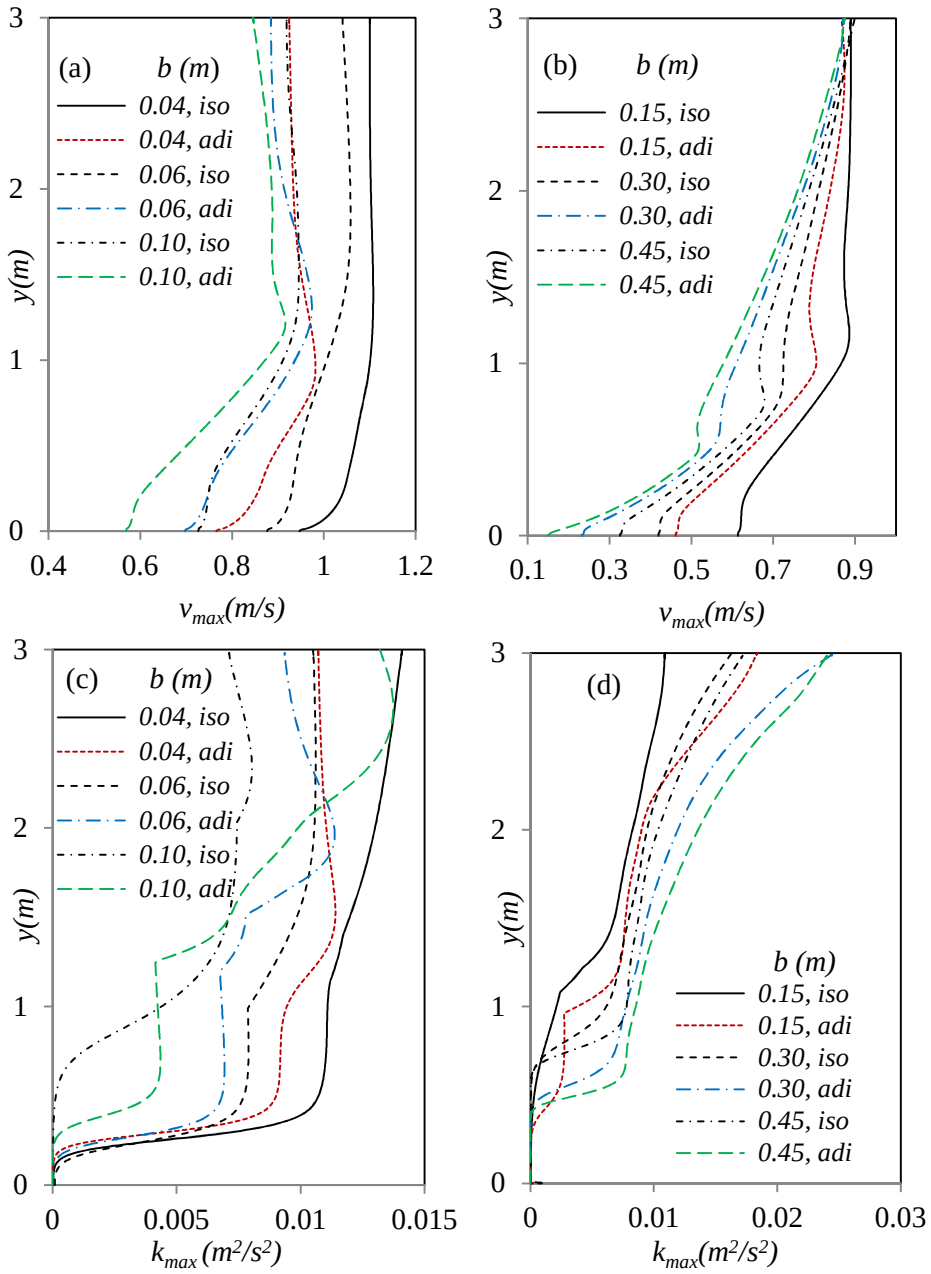

Figure 9 Comparison of the maximum velocity (a, b), kinetic energy (c, d) and turbulent intensity (e, f) between the isothermal (iso) and adiabatic (adi) cases.

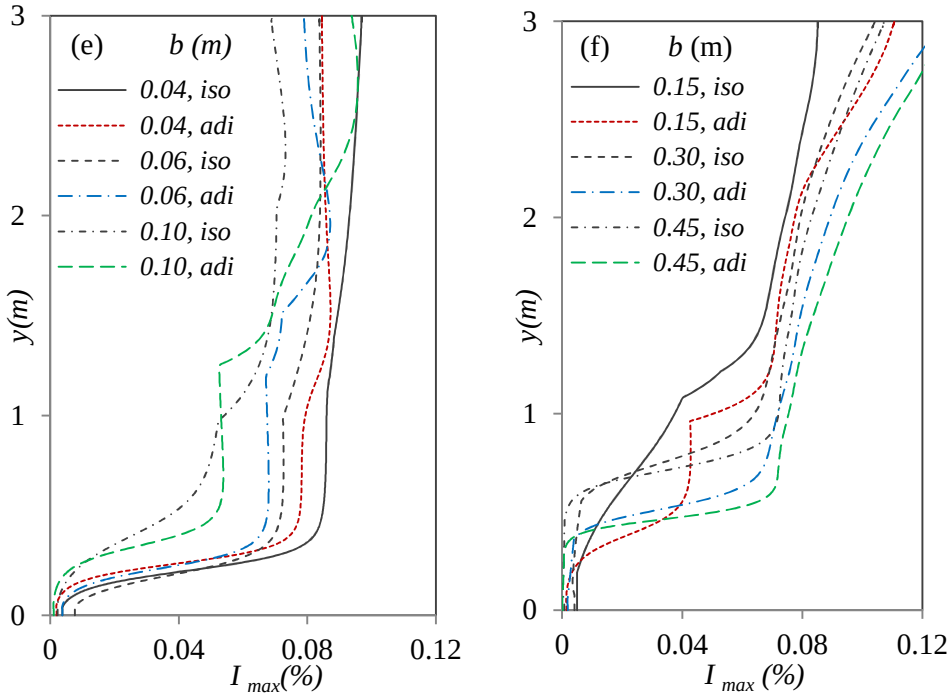

Figure 9 Caption continued.

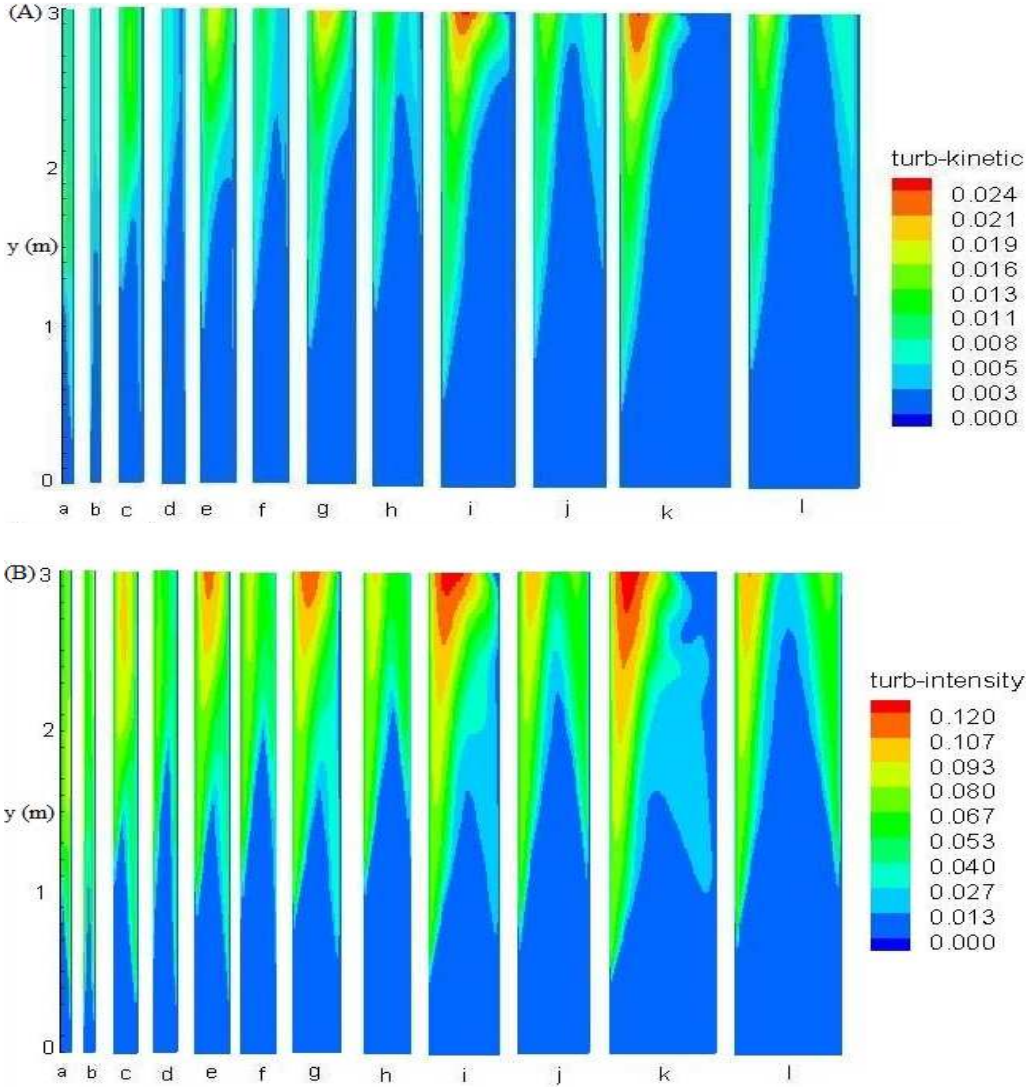

Figure 10 Contours of the turbulent kinetic energy (A), turbulent intensity (B) and velocity (C) at various channel width. Note the adiabatic results are in frames (a, c, e, g, i, k) while the isothermal are in (b, d, f, h, j, l).

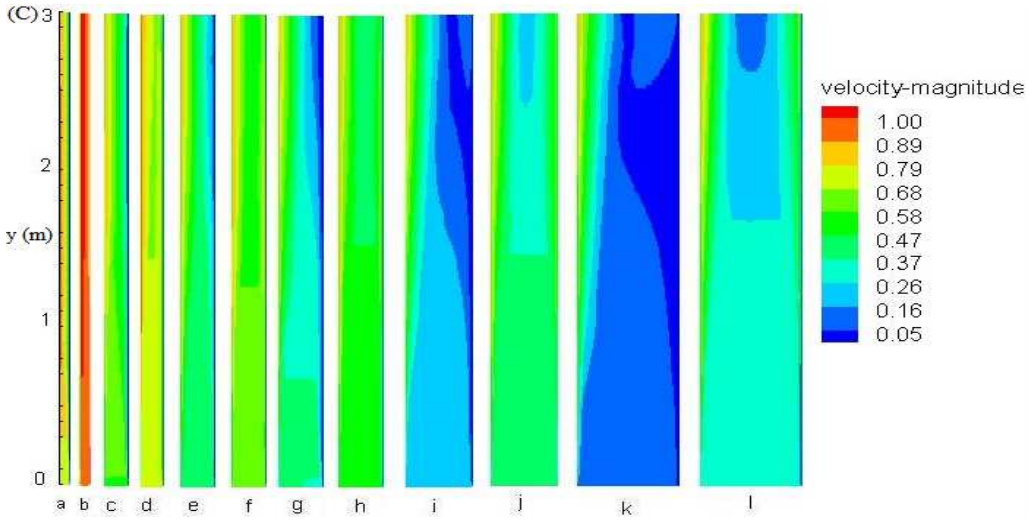

Figure 10 Caption continued.

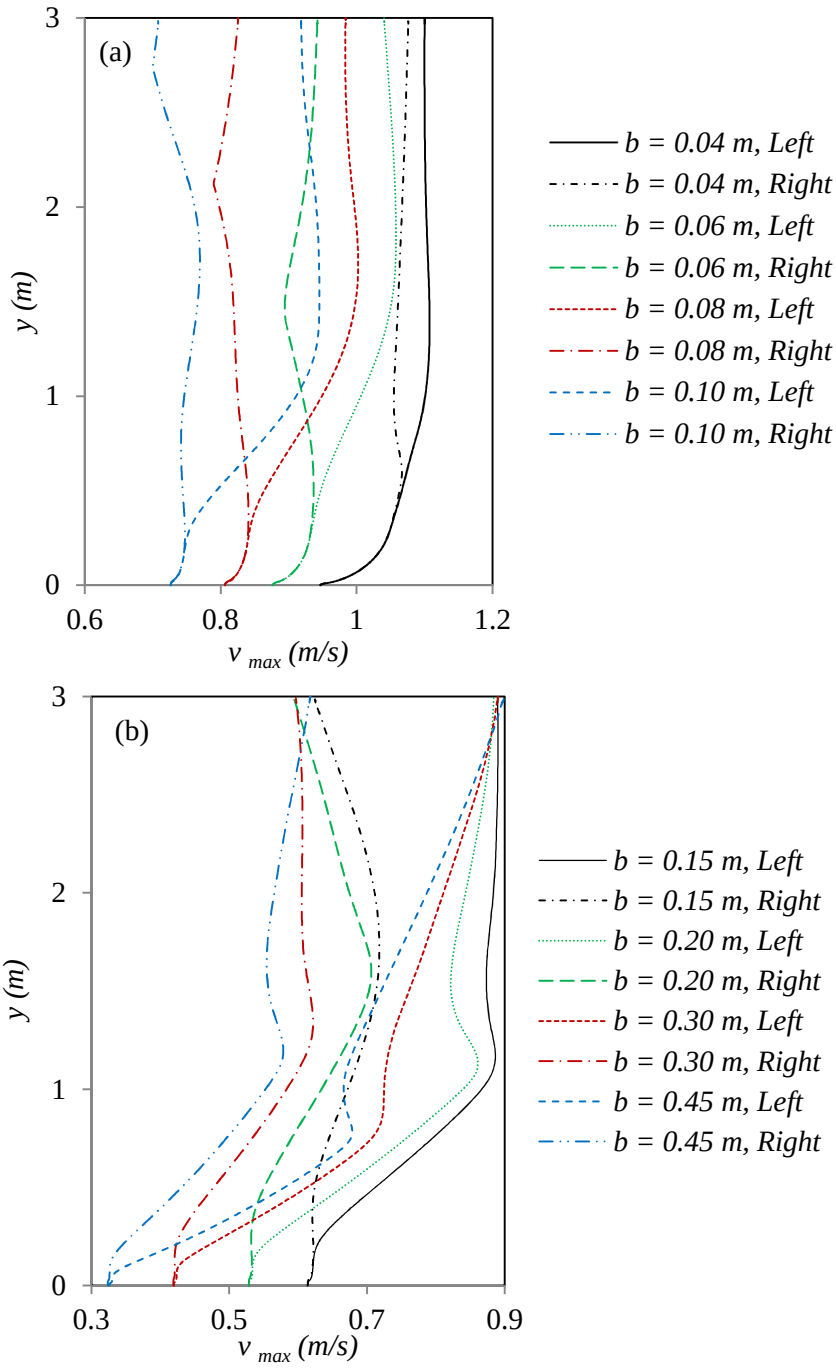

Figure 11 Comparison of the velocity predicted on the left and right sides of the channel at $Tp_{*} =$ 40°C.

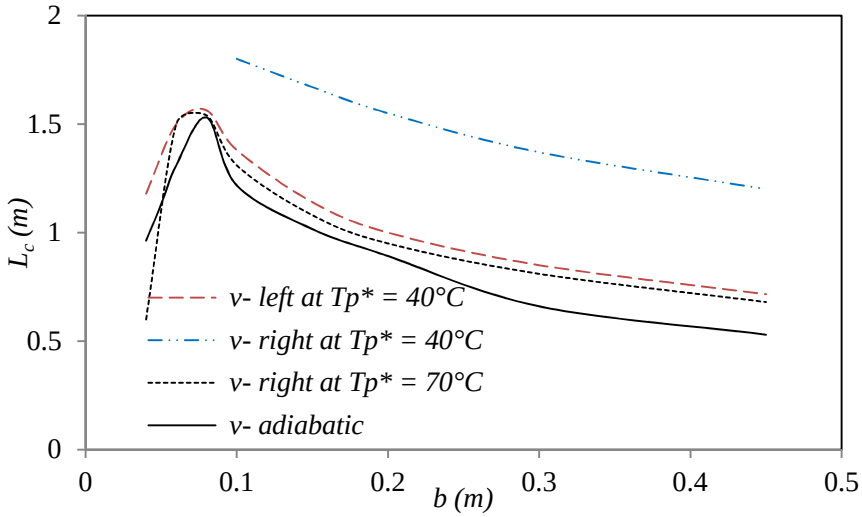

Figure 12 Critical distance of the flow transtion inside the channel.